

Computer-Assisted Orientation and Drawing of Archaeological Pottery

1
2

Q1

JOSEF WILCZEK, Université Bourgogne Franche-Comté, France and Masarykova Univerzita, Czech Republic
 FABRICE MONNA, AHMED JÉBRANE, and CATHERINE LABRUÈRE CHAZAL,
 Université Bourgogne Franche-Comté
 NICOLAS NAVARRO and SÉBASTIEN COUETTE, Université Bourgogne Franche-Comté, France and
 EPHE, PSL University, France
 CARMELA CHATEAU SMITH, Université Bourgogne Franche-Comté, France

Archaeologists spend considerable time orienting and drawing ceramic fragments by hand for documentation, to infer their manufacture, the nature of the discovery site and its chronology, and to develop hypotheses about commercial and cultural exchanges, social organisation, resource exploitation, and taphonomic processes. This study presents a survey of existing solutions to the time-consuming problem of orienting and drawing pottery fragments. Orientation is based on the 3D geometry of pottery models, which can now be acquired in minutes with low-cost 3D scanners. Several methods are presented: they are based on normal vectors, or circle fittings, or profile fittings. All these methods seek to determine the optimal position of the rotation axis. We also present and discuss new approaches and improvements to existing methods. We have developed a suite of functions for the computer-assisted orientation and drawing of archaeological pottery. The profile and contours of the fragment, as well as any possible decoration, can be depicted in various ways: photorealistic rendering or dotted patterns, calculated by ambient occlusion, combined or not with artificial light. The general workflow, evaluated using both synthetic and real-world fragments, is rapid, accurate, and reproducible. It drastically reduces the amount of routine work required to document ceramic artefacts. The information produced, together with the 3D representation of the fragments, can easily be archived and/or exchanged within the archaeological community for further research. The source code (built in the R environment), together with an installation notice and examples, is freely downloadable.

CCS Concepts: • **Applied computing** → **Archaeology**;

Additional Key Words and Phrases: Archaeology, documentation, (semi-)automatic pottery orientation, pottery illustration, 3D reconstruction

We are very grateful to the CNRS (BQR-PRES and PEPS HUMAIN grants) and SATT Grand Est for funding and material support.

Authors' addresses: J. Wilczek (Corresponding author), Université Bourgogne Franche-Comté, ARTEHIS - UMR CNRS 6298, 6 Bd Gabriel, Dijon, 21000, France, Masarykova Univerzita, Ústav archeologie a muzeologie, Arna Nováka 1, Brno, 60200, Czech Republic; email: josef.wilczek@hotmail.com; F. Monna, Université Bourgogne Franche-Comté, ARTEHIS - UMR CNRS 6298, 6 Bd Gabriel, Dijon, 21000, France; email: fabrice.monna@u-bourgogne.fr; A. Jébrane, Université Bourgogne Franche-Comté, IMB - UMR CNRS 5584, 9 av. Alain Savary, Dijon, 21000, France; email: ahmed.jebrane@u-bourgogne.fr; C. L. Chazal, Université Bourgogne Franche-Comté, IMB - UMR CNRS 5584, 9 av. Alain Savary, Dijon, 21000, France; email: catherine.labruere@u-bourgogne.fr; N. Navarro, Université Bourgogne Franche-Comté, Biogéosciences - UMR CNRS 6282, 6 Bd Gabriel, Dijon, 21000, France, EPHE, PSL University, 4-14 Rue Ferrus, Paris, 75014, France; email: nicolas.navarro@ephe.psl.eu; S. Couette, Université Bourgogne Franche-Comté, Biogéosciences - UMR CNRS 6282, 6 Bd Gabriel, Dijon, 21000, France, EPHE, PSL University, 4-14 Rue Ferrus, Paris, 75014, France; email: sebastien.couette@ephe.psl.eu; C. C. Smith, Université Bourgogne Franche-Comté, UFR SVTE, 6 Bd Gabriel, Dijon, 21000, France; email: carmel.chateau@laposte.net.

Permission to make digital or hard copies of all or part of this work for personal or classroom use is granted without fee provided that copies are not made or distributed for profit or commercial advantage and that copies bear this notice and the full citation on the first page. Copyrights for components of this work owned by others than the author(s) must be honored. Abstracting with credit is permitted. To copy otherwise, or republish, to post on servers or to redistribute to lists, requires prior specific permission and/or a fee. Request permissions from permissions@acm.org.

© 2018 Copyright held by the owner/author(s). Publication rights licensed to ACM

1556-4673/2018/11-ART22 \$15.00

<https://doi.org/10.1145/3230672>

ACM Reference format:

Josef Wilczek, Fabrice Monna, Ahmed Jébrane, Catherine Labrière Chazal, Nicolas Navarro, Sébastien Couette, and Carmela Chateau Smith. 2018. Computer-Assisted Orientation and Drawing of Archaeological Pottery. *ACM J. Comput. Cult. Herit.* 11, 4, Article 22 (November 2018), 17 pages.
<https://doi.org/10.1145/3230672>

1 INTRODUCTION

Pottery fragments are among the most abundant artefacts found during archaeological surveys and excavations. Together with their function, manufacture, and chronology, they provide evidence of human organisation, resource exploitation, and taphonomic processes [46, 51]. Recent developments in 3D computer graphics and pattern recognition have led to prominent advances in the treatment of archaeological pottery, aiming to provide semantic data-based systems, allowing the annotation, retrieval, and reassembly of pottery fragments, and predictive digitisation of vessels [8, 19, 38, 47–49, 68]. However, despite these advances, a practical and easy-to-use solution to the time-consuming problem of methodical archaeological illustration is still not readily available for the large-scale documentation of archaeological remains. Current archaeological illustrations are standardised, at least in part (see, e.g., [1, 9, 16, 18, 58, 60]). Archaeological pottery drawings are generally divided into two parts: the central line represents the axis of rotation, the left part depicts the vertical section with any inner details; the right part depicts the outer section. The position of the rotation axis, which is of primary importance for further classification, is traditionally defined by positioning the rim or base of the fragment on a radius chart. Once the fragment has been oriented and its diameter determined, the profile outline is obtained by a profile gauge, drawn manually in a cutaway view, then scanned and processed with graphical software to produce the final raster or vector image. Drawing pottery is thus a time-consuming and costly task, especially when dealing with hundreds or even thousands of fragments. Since the 1990s, numerous articles have been published on how to automate the orientation process (e.g., [34, 50]). Most methods exploit three fundamental geometric properties of rotationally symmetrical objects (Figure 1): (i) normal vectors of the surface pass through the axis of rotation (Figure 1(a); e.g., [4, 20–23]); (ii) horizontal planes intersecting the object form circles whose centres lie on the axis (Figure 1(b); e.g., [22, 32, 39, 40, 42]); and (iii) fragment profiles projected to the same vertical plane occupy the same location (Figure 1(c); e.g., [33, 34]). Note that the first two properties do not concern surfaces that are orthogonal to the axis, such as flat bases. Our goal here is therefore to inventory existing approaches for rotation axis estimation, based on normal vectors, horizontal/vertical sections, and to introduce new methods capable of segmenting fragments (outer and inner surfaces), and discarding parts that do not provide information about the rotation axis (fractures, plastic decoration, etc.). Most published studies have focused on theoretical aspects. The description of the algorithms used is often succinct and the code is not always available, so that it is difficult to replicate the procedures involved, for quantitative comparison. Rotation axis estimation has often been tested on only a few large, regular, well-preserved fragments. The final illustrations are frequently schematic, and do not necessarily integrate all the information about the fragment surface. Some authors have proposed practical tools or, at least, pipelines (e.g., [13, 52, 53]), but no multiplatform solution has so far been made available to the archaeological community, except to some extent the Gigamesh software (<http://www.gigamesh.eu> [41]), or intra-laboratory software, available upon request [34]. Note that these solutions are not yet complete; they do not cover all existing procedures, and/or do not always allow archaeological illustrations to be produced in conformity with current standards. We have developed approaches based on these existing state-of-the-art methods, adopting optimal procedures for each part of the process. The material and methods section therefore provides a detailed description of these proposed approaches. A fully automatized workflow (i.e., the most constraining) is tested on datasets consisting of both synthetic models and real-world archaeological fragments. Results are evaluated in terms of reproducibility and then compared with traditional illustrations produced by specialists. The new tools presented here for pottery orientation are freely available, as a suite of functions encoded in R software

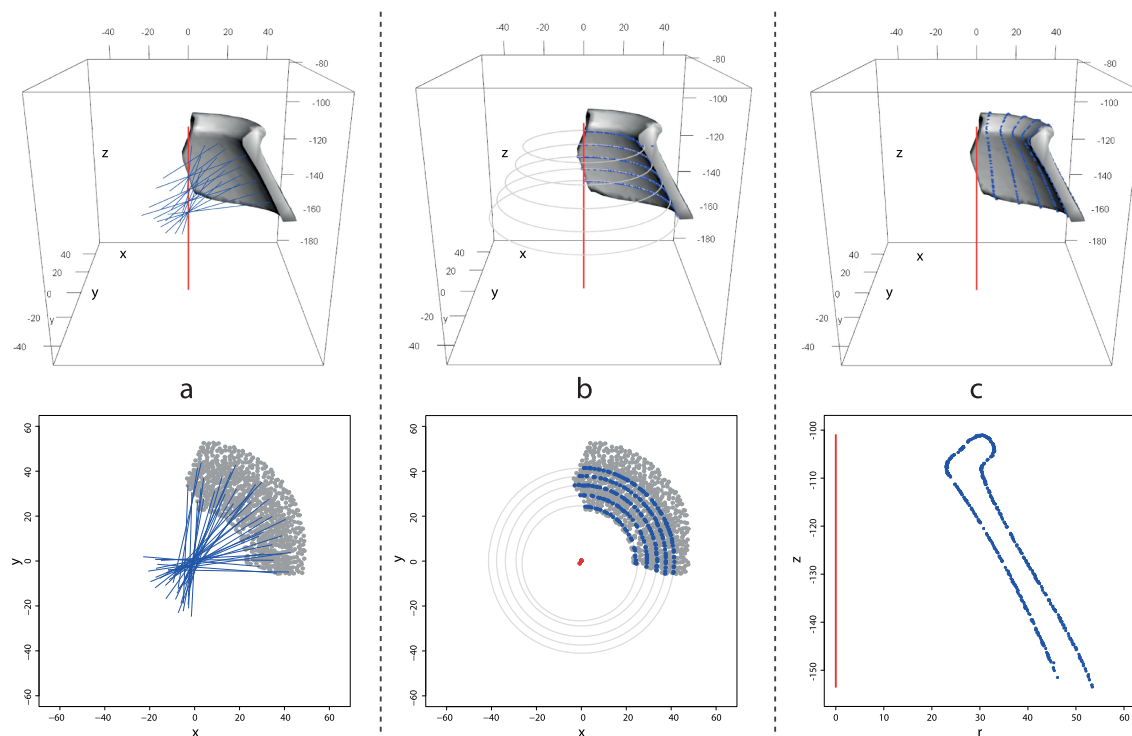


Fig. 1. Three main geometric properties of the rotationally symmetrical objects exploited for rotation axis estimation. (a) Normal vectors of vertices lying on the pottery surface pass through the axis of rotation. (b) Horizontal planes intersecting a fragment form circles whose centres lie on the rotation axis. (c) Fragment profiles projected to one plane occupy the same location.

[62], including the production of archaeological illustrations, adapted to most norms and standards of pottery drawings (linear and shaded drawing, photographic representation, etc.). A user-friendly interface is proposed, with many options and tuneable parameters, to address problems of illustration likely to be encountered by the archaeological community.

2 MATERIAL AND METHODS

2.1 Acquisition

The 3D model of the pottery fragment can be obtained by any method (CT scan, photogrammetry, laser scan, etc.), but a 3D scanning system based on structured light is a suitable choice at this step because of its rapidity, adequate accuracy, and simplified manipulation. For the present study, 110 pottery fragments (rim, body, and base), different in size, shape, and/or state of preservation, from three chronological periods (Neolithic, Bronze Age, and Roman), produced using various fabrication techniques, were scanned with an EinScan-S structured light-based 3D scanner (resolution $<100\mu\text{m}$). The entire acquisition process, including scanning and post-processing, took at most 5 minutes per fragment. Typically, the number of faces used for further calculation was limited to 500,000, which will allow further drawing of complex decoration, while keeping computation time to a minimum. In any case, possible defects of the model, such as duplicated or unreferenced vertices, or non-manifold faces, should be repaired prior to treatment. The synthetic data used to test the quality of automatic orientation was produced as follows. A 3D pottery model was created in the free Blender software (<https://www.blender.org/>)

22:4 • J. Wilczek et al.

by rotating the vectorised profile of a 30-cm-high vessel from the Bibracte *oppidum* (Burgundy, France) around its axis of rotation. As the resulting model was perfectly symmetrical, deformation and noise were applied to the surface, to better simulate real-life conditions. The reconstructed vessel was randomly broken into 34 pieces, using a Voronoi fracture diagram. All fragments were then rotated, translated, and shuffled in the 3D space, as the starting point of the experiment.

2.2 Model Pre-Orientation

A fragment can be pre-oriented either manually or automatically. As difficult-to-process 3D models usually contain a large number of vertices, Quadric Edge Collapse Decimation [15] was used to reduce the number of vertices to approximately 10,000. To lessen the influence of features containing no information about the rotation axis (e.g., decoration), we opted to smooth the model, using a Laplacian Smoothing algorithm [63].

2.2.1 Manual Pre-Orientation. Manual pre-orientation exploits the fact that an expert is often intuitively able to pre-orient the fragment simply by perceiving its overall shape, or by identifying some specific horizontal features (e.g., rim, base, wheel-thrown lines on the inner side of fragment, horizontal decoration). Three points can then be defined within the same horizontal plane. The centre of the circle passing through these three points is determined using least-squares fitting [6]. The model is shifted and rotated to make the rotation axis coincide with the z -axis of the orthonormal coordinate system (Figure 2). All parts with normals that do not point to the rotation axis (i.e., fracture surfaces, handles, plastic decoration, base, and rim), must be removed. Pertinent surfaces are then extracted by first calculating the distance, $d(n_i, Z)$, between the straight line n_i defined by each vertex X_i and its corresponding normal vector \vec{N}_i , and the rotational axis Z defined by $X_0 = [0, 0, 0]$ and $\vec{N}_0 = [0, 0, 1]$ (Equation (1); [20, 21]):

$$d(n_i, Z) = \frac{(X_i - X_0) \cdot (\vec{N}_i \times \vec{N}_0)}{\|\vec{N}_i \times \vec{N}_0\|}. \quad (1)$$

In our approach, only the points presenting the lowest distances (e.g., 50%) were retained, as these points contain sufficient information for pre-alignment. It is then fairly straightforward to separate the inner and outer surfaces of the model by examining whether a vertex shifted by its normal is closer to the rotation axis or not.

2.2.2 Automatic Pre-Orientation. Automatic model pre-orientation in our approach consists of two steps: (i) elimination of vertices that are not part of the surface of revolution; and (ii) estimation of the rotation axis by normal vectors, using robust regression. Vertices located on non-regular features (i.e., fracture surfaces or plastic decoration) do not belong to the surface of revolution, and must therefore be discarded. As opposing vessel surfaces are approximately parallel, the normal vectors (e.g., \vec{N}_i and \vec{N}_i') of two vertices (e.g., X_i and X_i') lying exactly opposite each other should point in opposite directions (Figure 3(a)). The probability, p , that any two normal vectors point in opposite directions was evaluated following Li [37] and Schlager [56, 57], and only those vertices, X_i , where the vectors have a p value higher than a defined threshold value (e.g., 0.95) were retained. After eliminating vertices that are not part of the surface of revolution, the automatic pre-orientation process then seeks a line (i.e., the axis of rotation) for which the sum of the squared distances to normals is minimal (Figure 1(a)). Two approaches exist for this process: the Hough Transform, by tracing normals through the accumulator space (e.g., [23, 27, 28, 66]), and direct least-squares optimisation (e.g., [20–22]). This second approach has often been thought to lack robustness (e.g., [42]), but a modified version was successfully applied here. As demonstrated by Halíř [20, 21], the position of the vertex (X_0) on the estimated axis in Equation (1) is linearly related to the normal vector direction of the axis (\vec{N}_0). The search for the axis of rotation can therefore be simplified as a two-parameter optimisation problem (calculated here by the Nelder-Mead algorithm [44, 45]): φ for rotation around the x -axis and θ for rotation around the y -axis (see [20, 21] for more details). To improve the robustness of Halíř's approach, the X_0 coordinates were calculated using very robust linear regression [43,

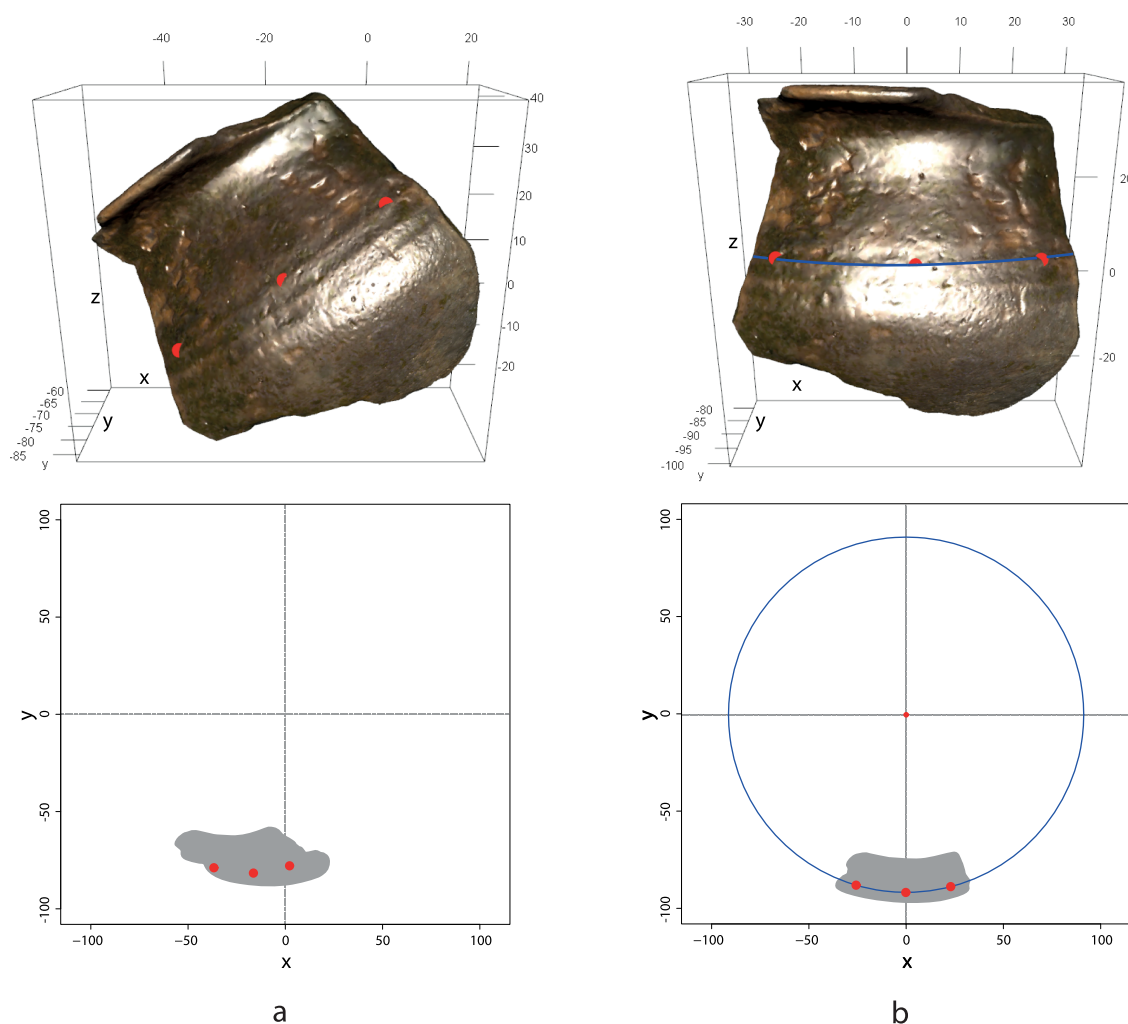


Fig. 2. Manual pre-orientation. (a) Three points (red dots) defined on the model. (b) The model is rotated by the plane defined by the three points, and a circle (blue line) is then fitted to the three points. The model is then shifted along the x - and y -axes to coincide with the rotation axis.

67], after the elimination step. This method is expected to considerably reduce the deleterious impact of outliers among the normal vectors, or any other source of data noise. The model is rotated and translated, once φ and θ have been calculated, so that its axis of rotation coincides with the z -axis. The inner and outer surfaces can then be separated, as described in the manual pre-orientation paragraph above (Section 2.2.1).

2.3 Fine-Tuning the Axis of Rotation

Several methods have been proposed to improve the position of the rotation axis. In our approach, the surface choice option (inner, outer, or both) allows the more regular surface to be selected.

2.3.1 Horizontal Circle Adjustment Using the Radius. For an idealised fragment, properly oriented along the z -axis, the horizontal planes intersecting the inner and outer surfaces should form perfect circles (Figure 1(b)).

22:6 • J. Wilczek et al.

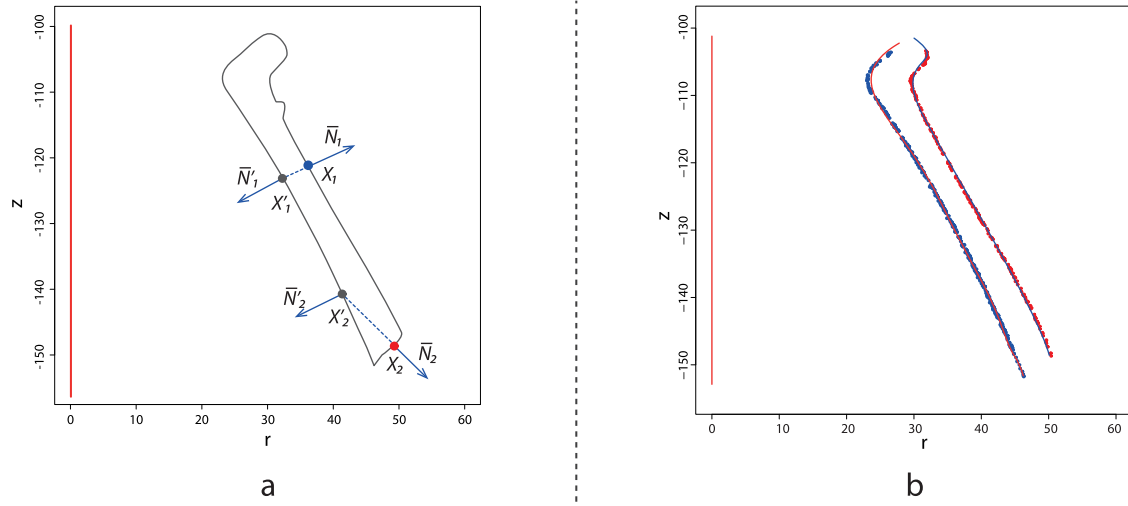


Fig. 3. Extraction of surfaces relevant to axis estimation (a) and vertical profile superimposition using polynomials (b). (a) Vertex lying on parallel (blue dot) and non-parallel (red dot) fragment surfaces. (b) Fragment vertices of inner (blue dots) and outer (red dots) surfaces are perfectly superimposed and adjusted to the corresponding polynomial (red and blue curves).

134 For a real-world object, the distance between all vertices belonging to the same section and the rotation axis,
 135 $d(X_{i,j}, Z)$, should thus be as constant as possible. It is therefore a matter of minimising the mean variance of
 136 these distances, as follows (Equation (2)):

$$\min_{\varphi, \theta, a, b} \left(\sum_{i=1}^K \frac{1}{k_i} \sum_{j=1}^{k_i} [d(X_{i,j}, Z) - \overline{d(X_{i,j}, Z)}]^2 \right), \quad (2)$$

137 where a , b , φ , and θ translate and rotate the model to make it coincide with the rotation axis, K is the number of
 138 horizontal sections, and k_i the number of points in the i -th horizontal section. The minimisation function here
 139 requires the optimisation of four parameters (φ , θ , a , and b). However, the search process can be performed with
 140 only two parameters (a and b), to keep the three points set for manual pre-orientation on the same horizontal
 141 plane.

142 **2.3.2 Horizontal Circle Adjustment Using the Multi-Criteria Approach.** In addition to the property stated in
 143 Section 2.3.1., the centres of circles previously calculated and projected onto the xy -plane should all be super-
 144 imposed on the rotation axis (Figure 1(b); e.g., [21, 22, 32, 34, 42, 54]). These two criteria can be treated simulta-
 145 neously, using a multi-objective optimisation procedure (also known as Pareto). However, as the calculation of
 146 the circle centres by least-squares fitting is sensitive to the sector angle, in our approach, its value was used to
 147 weight both cost functions (note that a minimum number of points and minimum sector angle can be specified
 148 in advance). The first (objective) cost function minimises the variability of the circle centres projected onto the
 149 xy -plane (Equation (3)):

$$\min_{\varphi, \theta} \left(\frac{1}{\sum_{i=1}^K w_i} \sum_{i=1}^K w_i d(C_i, \bar{C})^2 \right), \quad (3)$$

150 where C_i is the centre of the optimal circle obtained by regression from points belonging to the i -th horizontal
 151 section, and \bar{C} gives the mean coordinates of these centres. The weight, w_i , is the value of the sector angle
 152 expressed in radians. The second cost function minimises the mean-squared distances between each point and

its corresponding circle centre (Equation (4)):

153

$$\min_{\varphi, \theta} \left(\frac{1}{\sum_{i=1}^K w_i} \sum_{i=1}^K \frac{w_i}{k_i} \sum_{j=1}^{k_i} [d(X_{i,j}, C_i) - R_i]^2 \right), \quad (4)$$

where R_i is the radius of the regression circle. With this approach, the translation parameters a and b no longer integrate the optimisation process. Once φ and θ have been determined, a and b are straightforwardly drawn from the mean circle centre (\bar{C}). As the model is already pre-oriented, the search process for φ and θ can be limited (e.g., $\pm 10^\circ$), rather than searching within the entire solution space. The Pareto front represents a set of optimal non-dominated solutions in a simple two-dimensional graph, where both x - and y -axes correspond to both objectives. From the visual inspection of this graph, it is possible to decide which solution (or average of a set of solutions) is the most convenient [11], or to select one objective rather than the other, depending on the fragment.

154
155
156
157
158
159
160
161

2.3.3 Vertical Profile Superposition. The profiles corresponding to the intersection of the vertical planes passing through the rotational axis and the fragment, projected onto the rz -plane (where r is the radius) should be superimposed (Figure 1(c); e.g., [29, 33, 34]). In our approach, the longest profile was first set as reference, and the optimal position was obtained when the sum of squared distances between the vertices of the reference profile and those of the other profiles was minimal (Equation (5)):

162
163
164
165
166

$$\min_{\varphi, \theta, a, b} \sum_{i=1}^M \left(\min_{\rho_j, \zeta_j} \left((r_i - \rho_j)^2 + (z_i - \zeta_j)^2 \right) \right), \quad (5)$$

where M is the total number of vertices, (r_i, z_i) the rz -coordinates of the points, and (ρ_j, ζ_j) the rz -coordinates of the reference section. Note that this method can be applied to the entire profile. The inner and outer reference profiles can also be considered as polynomial functions. In an ideal case, all vertices projected onto the same rz -plane should perfectly fit these curves (Figure 3(b) [64, 65]). The optimal position of the model is found by minimising the sum of squared residuals between vertices and reference polynomial functions, $f(z_i)$ as in Equation (6).

167
168
169
170
171
172

$$\min_{\varphi, \theta, a, b} \sum_{i=1}^M (r_i - f(z_i))^2. \quad (6)$$

2.3.4 Tangent Plane to Rim and Base. This method uses the traditional principles by which the specialist orients fragments: the optimal orientation is found when the rim/base vertices coincide with the horizontal plane, and the axis of rotation is a line perpendicular to the centre of the circle passing through these vertices [34]. The rim (base) vertices are selected as those presenting the highest (lowest) z -values within each vertical section, and their distance to a horizontal plane is minimised (Equation (7)):

173
174
175
176
177

$$\min_{\varphi, \theta, a, b} \frac{1}{\sum \delta_j} \sum_{j=1}^L \delta_j (z_j - \max z)^2, \quad (7)$$

where L is the number of vertical sections and z_j is the z -coordinate of the point (for base fragments, $\min z$ is used instead of $\max z$). The number δ_j is equal to 1 if $|z_j - \max z| < \epsilon$ (e.g., 3 mm), or equal to 0 to eliminate inappropriate points (e.g., when the rim or base of the fragment is damaged).

178
179
180

2.3.5 Oriented Model Exportation. The final oriented model, produced using any of the above approaches, can be exported in Polygon File Format (PLY), and can be used for archaeological illustration, or 3D reconstruction.

181
182

22:8 • J. Wilczek et al.

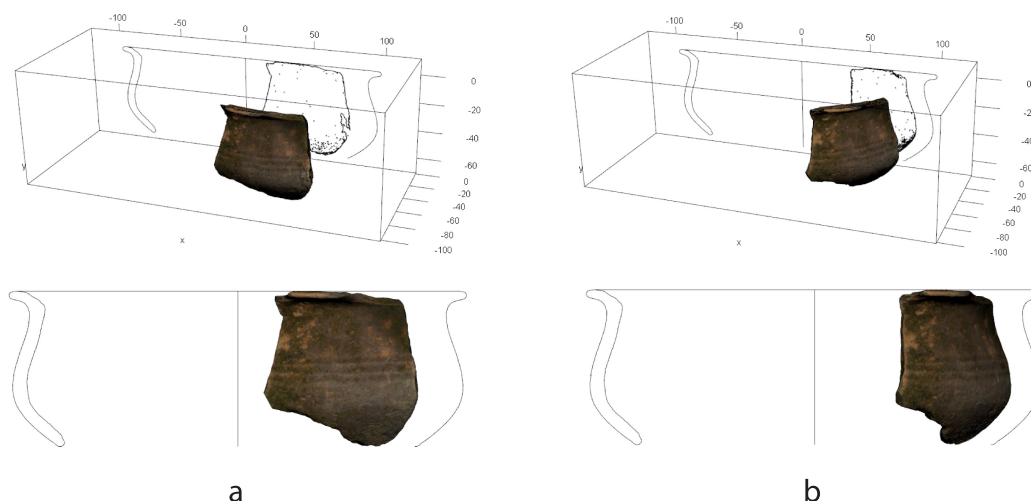


Fig. 4. Different options for fragment orientation used in illustration.

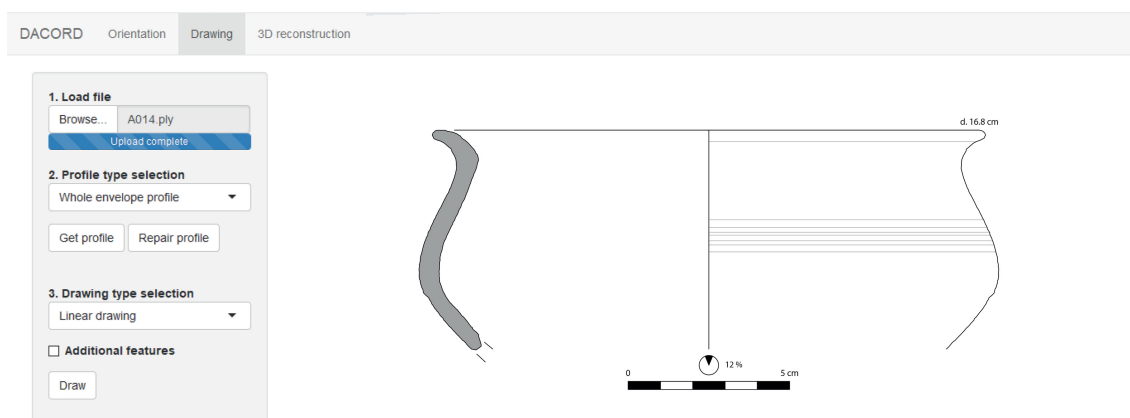


Fig. 5. Example of linear drawing illustration.

2.4 Archaeological Illustration

2.4.1 General Layout. Layouts are represented in the xz -plane, with the rotation axis coinciding with the z -axis. Fragments are traditionally depicted in front view, to the right of the rotation axis, with no consideration for its real geometric position (Figure 4(a)). Nevertheless, the fragment may be positioned in relation to the axis of rotation (Figure 4(b)), or rotated, for example, to depict a specific feature, such as a handle. Note that, at this step, the models were processed in full resolution, using the orientation parameters calculated above from their decimated representation.

2.4.2 Overall Form. The selected profile section is the longest part that contains enough information for further fragment classification (e.g., rim, foot, handles). Specific features can be included in the drawing, such as scale, distance measurements, volume estimation, maximum sector angle (a proxy for vessel preservation), prolongation of the missing profile parts, and horizontal lines (Figure 5).

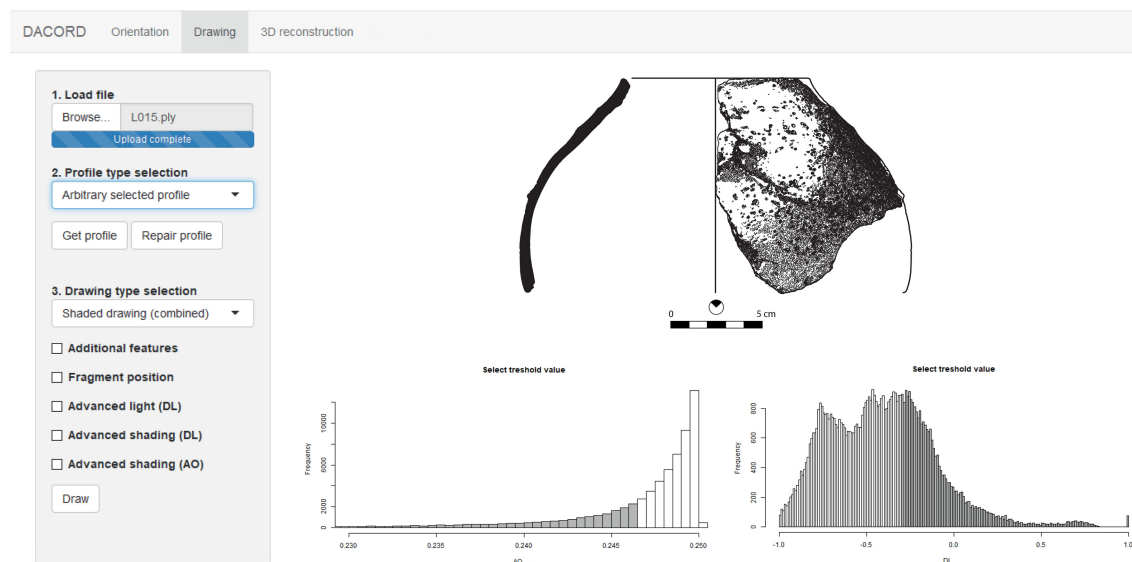


Fig. 6. Example of shaded drawing using a combination of directional lighting and ambient occlusion. Values in distributions used for fragment shading are highlighted in grey.

2.4.3 Fragment Rendering. In modern archaeological illustrations, the fragment surface is increasingly represented through colour/greyscale photography. To obtain such illustrations, the colour or greyscale values of the vertices/faces are projected orthogonally onto the xz -plane (Figure 4; see also [60]). Dotted shading, to give a sense of depth to the drawing, may be used as an alternative. Calculations of the amount of light that a surface receives, and ambient occlusion, which indicates how much ambient light a point receives [25], can be found in most textbooks (e.g., [14]). Ambient occlusion darkens the more occluded points of the 3D model, creating a more realistic appearance [36]. Here, the package *shadevis* written in C++ (<https://sourceforge.net/projects/vcg/files/shadevis/>) and used via Meshlab [7] was preferred, because it produces satisfactory results rapidly. Shading was rendered by plotting more dots in the darkest areas (Figure 6).

2.4.4 Vessel Regularity. Once aligned, possible irregularities in the surface, such as decoration or technological traces, can be revealed by two visualisation methods. The first calculates the distances between model points and the rotation axis, and depicts them on the model surface using a colour code (Figure 7(a)), so that points belonging to the same horizontal section should ideally have the same colour. In the second method, the distance is measured between model points and the corresponding ideal vessel, obtained by rotating a model profile around the rotation axis (Figure 7(b)). A regular model should thus appear as homogeneously coloured as possible (here, in blue corresponding to values close to 0). These representations also illustrate the quality of fragment orientation.

2.4.5 3D Reconstruction of the Preserved Part of the Vessel. Turning one of the profiles along the rotation axis produces a 3D reconstruction of the vessel (Figure 7(b); e.g., [3, 30, 41]).

2.4.6 Illustration Exportation. All archaeological illustrations produced can be exported in Encapsulated PostScript format (EPS), while oriented models and 3D reconstruction obtained by revolution around the rotational axis can be exported as a triangular mesh (in PLY format).

22:10 • J. Wilczek et al.

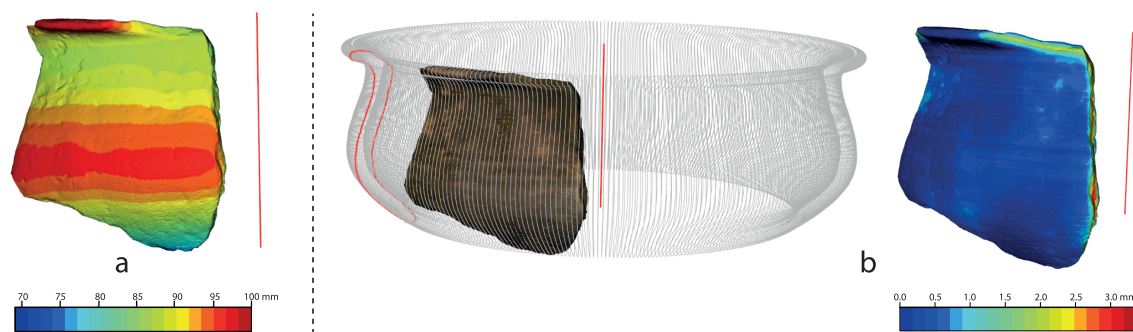


Fig. 7. Two methods of calculating vessel regularity: (a) Distances between model points and the axis of rotation. (b) Distance between the model (in brown) and the corresponding ideal vessel (in grey), obtained by rotating a given model profile (red polygon), around the axis of rotation.

2.5 Programming and Distribution

The suite of functions written in the R environment, together with instructions and examples, are freely available as Supplementary Materials S1. The functions use several packages for calculation, and the Shiny application framework [5], combined with RStudio [61], providing a user-friendly graphical interface, which does not require any particular knowledge of computer coding. The full list of packages with corresponding references is provided in Supplementary Materials S2. It should be noted that all software and packages used are freely available.

3 RESULTS

3.1 Evaluation of the Workflow On a Synthetic Model

A consumer-grade computer (Intel Core i7-2670QM - 2.20GHz, 8 Go DDR3, NVIDIA GeForce GTX 560M) was used for all the following experiments. Although alignment can be achieved in multiple ways, it was decided to evaluate the quality of the rotation axis position using the least restrictive procedure: the fully automatic pre-orientation via normals, with adjustment refining using the radius of the horizontal circles (performed on both inner and outer model surfaces, with $K = 20$ sections). The time required to process one fragment was less than 3 minutes. Once the rotation axis had been estimated for each fragment (Figure 8(c)), it was then automatically placed as close as possible to its original position, by minimising the mean point-to-point distance between the oriented fragment and the original. Note that, at this step, only translation along the z -axis, and rotation around it, were allowed, so that the quality of the rotation axis position was not affected (Figure 8(d)). Results showed that 29 fragments (85%) were well oriented, with a mean point-to-point distance not exceeding 4 mm (Figure 8(e) and (f)). This value may appear high, but it should be kept in mind that the original vessel was 30 cm tall, and that it had been severely deformed. The five unsatisfactory results concerned extremely small fragments, with flat bases, and/or possessing a sector angle too low to be properly treated. These fragments, which would undoubtedly have been discarded by the archaeologist as untreatable, demonstrate the limits of the fully automated method.

3.2 Evaluation of the Workflow On Real-World Pottery Fragments

All fragments were automatically oriented, as described in the previous paragraph. The distance between each oriented model and its corresponding ideal vessel (Figure 7(b)) was used as a proxy for orientation quality. For the vast majority of fragments ($n = 85$), the axis of rotation was determined almost perfectly, as the distances never exceeded 2mm (Figure (9), 1–10; for all results see Supplementary Materials S3). The normal-based pre-orientation failed for the 25 remaining fragments (Figure (9), 11–20), because they were small (e.g., Figure (9),

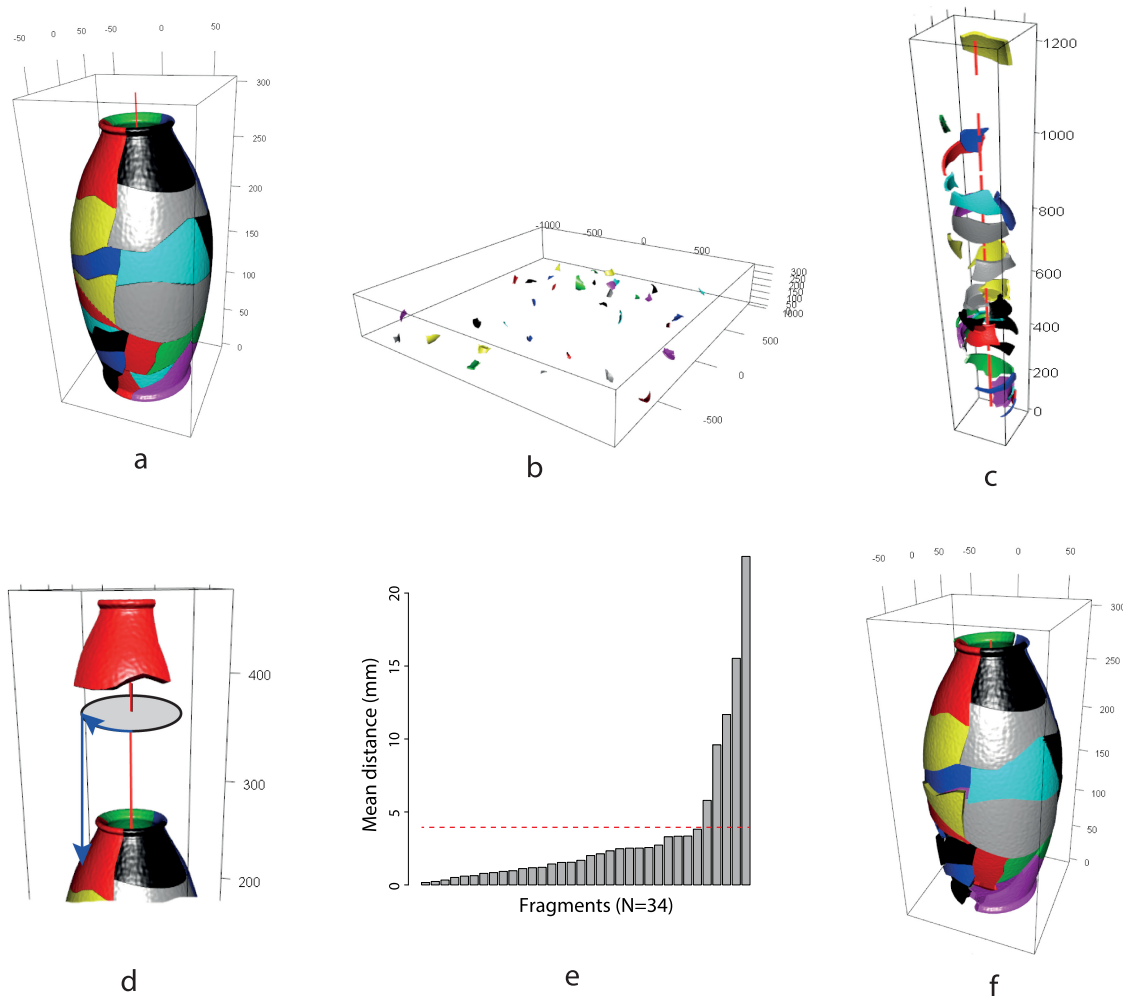


Fig. 8. Evaluation of the automatic workflow on a synthetic vessel. a) Synthetic vessel broken into 34 fragments. b) Randomly translated and rotated fragments. c) Fragments oriented by the system. d) Placing an aligned fragment in its original position on the vessel. e) Mean point-to-point distances between original and aligned fragments. f) Resulting aligned fragments.

11–12), almost flat (e.g., Figure (9), 13–14), they had too great a surface parallel with the rotation axis (e.g., bases 245
or rims; Figure (9), 15–17), or they were almost spherical (e.g., Figure (9), 18–20). However, most of these frag- 246
ments unsuitable for automatic pre-orientation due to their geometry can be processed with rapid manual pre- 247
orientation, simply by placing three points on the same horizontal plane (see results with manual pre-orientation 248
in Supplementary Materials S3–6). Even for nearly spherical body fragments, the presence of rills may also allow 249
the archaeologist to find a plane perpendicular to the rotation axis, thus making manual pre-orientation possible. 250

To test the robustness of the alignment procedure, an additional set of six rim fragments was processed by 251
four archaeologists, using different procedures for pre-orientation and final adjustment. Calculated rim radii 252
were then compared to those obtained by an expert in archaeological illustration (Table 1). The resulting values 253
were very similar whatever the operator and method. The calculated radii differed by less than 13% from those 254
determined by the expert (handmade and computer-made drawings are available in Supplementary Materials 255

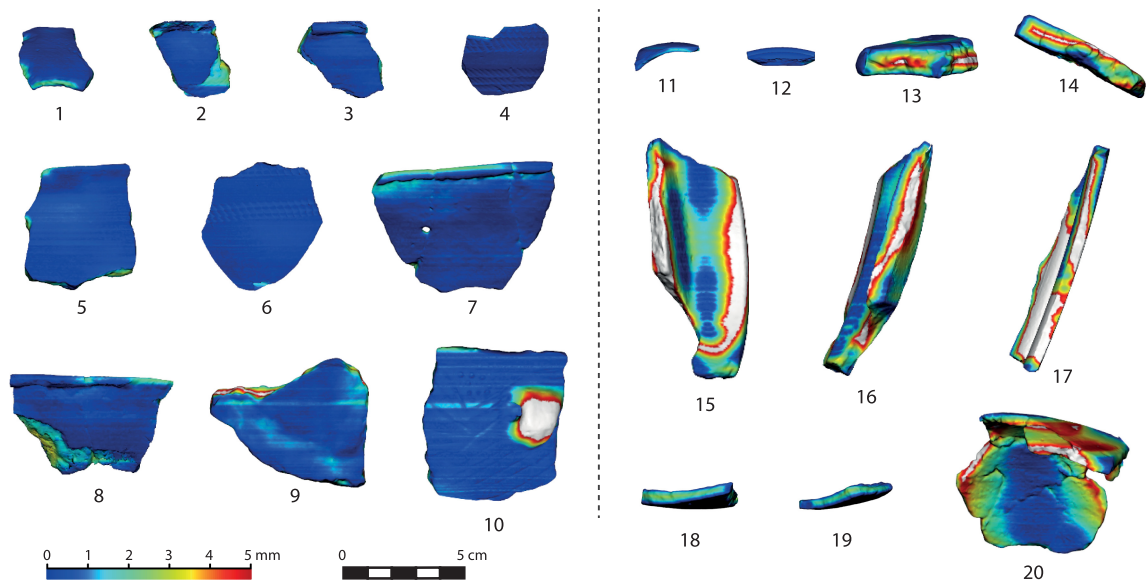


Fig. 9. Evaluation of the automatic workflow on real-world pottery fragments. (1–10) Example of well-oriented fragments. (11–20) Example of incorrectly oriented fragments. See Supplementary Materials S3 for more examples.

Table 1. Comparison of the Radius of Six Fragments, Determined (i) by an Expert Using Traditional Tools (Radius Expert Column) and (ii) by Four Archaeologists Using Different Procedures of Pre-Orientation and Final Adjustment (R1–4 Columns)

Fragment number	Sector angle	Radius expert (cm)	R1 (cm)	R2 (cm)	R3 (cm)	R4 (cm)	Range (cm)	sd (cm)
3077.22	9°	10.00	9.55	9.10	9.30	9.20	0.45	0.19
3077.35	12°	7.25	7.10	7.15	7.00	7.00	0.15	0.08
3077.42	7°	12.25	-	12.50	-	12.70	0.20	0.14
3107.08	13°	9.25	10.20	10.15	9.90	10.05	0.30	0.13
3107.25	10°	11.00	11.45	11.80	-	11.75	0.35	0.19
3107.26	18°	5.00	5.05	4.95	4.35	4.35	0.70	0.38

The sector angle provides information about fragment preservation. Range and standard deviation (sd) were calculated for the R1–4 Values. Corresponding drawings are available in Supplementary Materials S4.

S4), which are themselves subject to possible errors. Note that over half of the selected fragments had a sector angle of less than 12°, yet even for these difficult cases, satisfactory results were obtained.

As a demonstration of assisted drawing, a set of fragments was represented in linear mode (Figure (10), 1–2), coloured mode (Figure (10), 3–4), shaded modes using directional lighting and/or ambient occlusion (Figure (10), 5–8), and in a mode representing vessel regularity (Figure (10), 9–10). These illustrations possess the qualities required for archaeological documentation. Directional light shading highlights the overall vase relief, and any technological, plastic, or curved features (traces, ribs, mouldings, grooves, decoration, etc.). Ambient occlusion reveals local structure, but also fractures, defects, and surface porosity (Figure 6), independent of the light source position. In less than 5 minutes, the combination of all these illustration techniques produces results encompassing the most visible aspects of the pottery fragments. The 3D reconstruction of real-world pottery fragments was obtained in a few seconds (see Supplementary Materials S5).

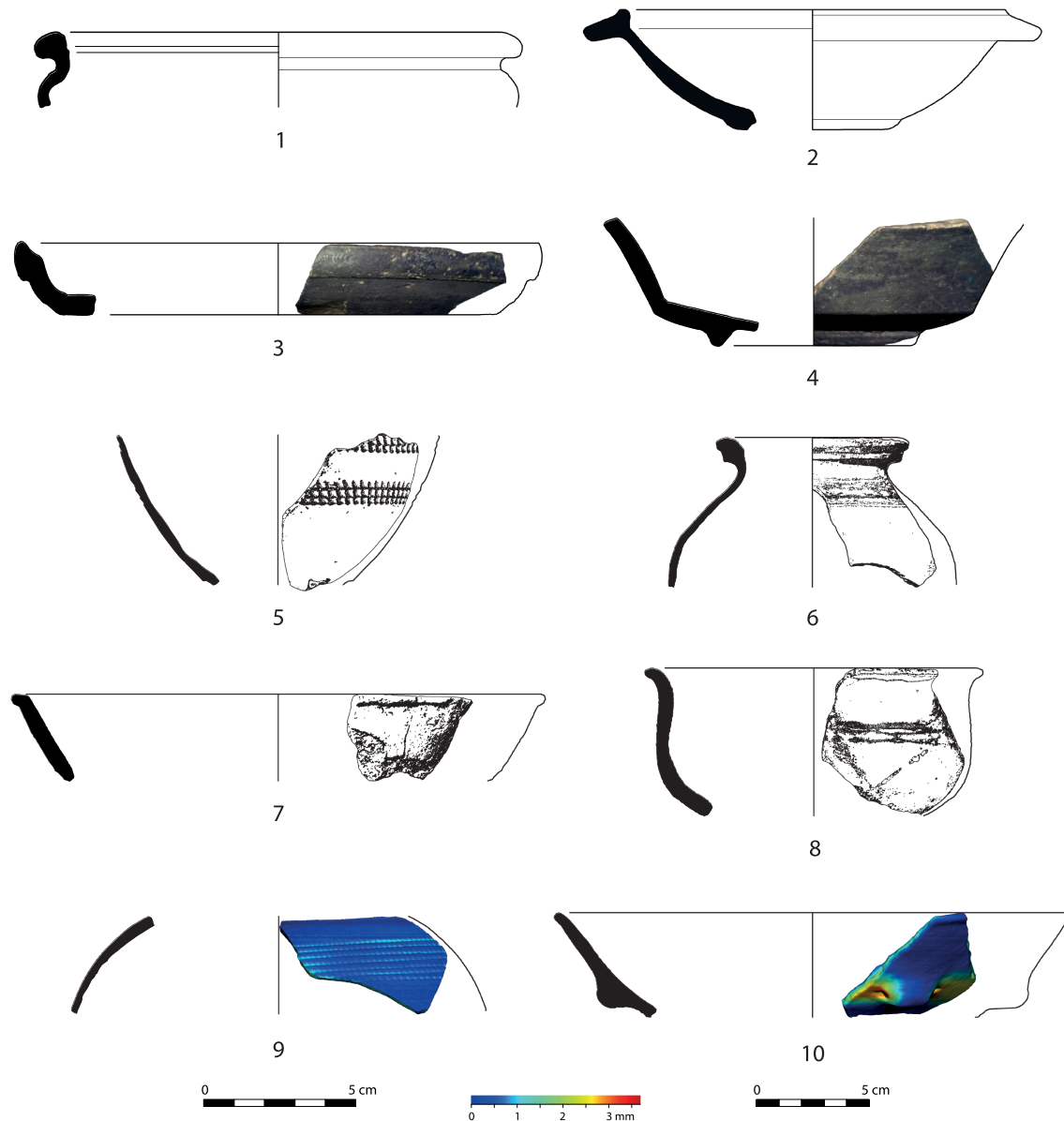


Fig. 10. Examples of archaeological illustrations. (1–2) Linear mode. (2–3) Colour mode. (5–8) Shaded mode. (9–10) Vessel regularity mode.

4 DISCUSSION

267

4.1 Strengths and Limitations of Orientation Methods

268

Although the specialist is usually able to sketch the profile of a fragment quickly, without any 3D modelling and subsequent extra time and cost, it is reasonable to expect that this 3D technology will soon be simplified, and available to the general public, as was the case for photography in its time. The low-cost 3D acquisition device

269

270

271

used here is quick to operate (ca. 5 min), and sufficiently accurate for ceramic studies. Generally, fragment size does not play a key role in the orientation of fragments, except when they are so small that the number of points is not sufficient for adequate processing. What matters more is the sector angle. Neither flat bases nor spherical fragments can be oriented automatically because all normals are parallel with the rotation axis, or they converge to a single point, producing an infinite number of solutions [34, 65]. Our approach was generally able to find the optimal rotation axis even for irregular hand-turned pottery, and for small fragments that would have been discarded by a skilled archaeologist. This result may considerably increase the quantity of data available for further archaeological interpretation. If enough fragments are well oriented, the possibility of automatic reassembly is greatly increased because their position with respect to the original rotational axis will provide a strong constraint (e.g., [10]). Sometimes the optimal orientation defined by 3D model geometry may differ from that preferred by ceramic specialists (e.g., Figure (9), 1–2, 7–8; Figure (10), 3, 7, 10). This is often true for upper parts, where the rim is traditionally fitted to a horizontal plane, perpendicular to the rotation axis (e.g., [2, 12, 26]). This strategy supposes that the potter created vessels with perfectly regular rims. Nevertheless, even wheel-turned pottery rarely satisfies this requirement, because centrifugal force considerably handicaps the potter's effort to keep the upper part of the vessel perfectly regular. Differences with traditional orientation decisions may also be seen when fragments contain decorations that are not perfectly horizontal, but that would naturally have been used to orient the vessel (e.g., Figure (9), 6; Figure (10), 5). Considering the variability of ancient production and post-depositional processes, every pottery fragment should be considered unique, and thus deserving of special attention. Should symmetry and overall 3D geometry, decoration, or rims be preferred for pottery orientation? The suite of functions proposed here allows all existing orientation solutions to be explored, but the final choice remains that of the archaeologist.

4.2 Quality of Archaeological Documentation

The pottery illustrations conform to current drawing norms. The shading tools can produce a detailed, very realistic, visual representation of the fragment surface, including most of its visible features. The vessel regularity representation provides a reliable estimate of orientation quality, and can also be used to study pottery-making tradition and specialisation. If required, illustrations can be modified in any graphical software. Profiles extracted can also be used for automatic classification of fragments based on their profile geometry (e.g., [17, 24, 29, 31, 35, 55, 59]). Profiles, illustrations, and models can also be integrated into existing databases and ongoing projects (e.g., ArchAIDE [19]; GRAVITATE [49]). Adding a third dimension to profiles augments the sense of depth, enhancing visual perception of their original shape, volume, and function. The greatest advantages of the suite of functions presented here are the gains in terms of time and amount of information obtained. The aim is for archaeologists to be less hampered by routine tasks. Pottery drawing based on 3D models may advantageously replace traditional tools, such as the stylus, profile gauge, and radius chart. The documentation produced is optimised for sharing (electronically or in paper format), presentation, and archiving. It can be further consulted for morphological, stylistic, or technological classifications. Besides these possibilities, the 3D models can be included in virtual reconstructions, developed in museography, education, or in the entertainment industry. These reconstructions can also be reproduced by 3D printers in a variety of materials (resin, plastic, ceramics, metal, etc.), and serve for exhibition, in place of plaster, as a support medium for the original fragments.

5 CONCLUSION

The suite of functions proposed here allows the expert to choose between several modern computational methods to determine the position of the rotation axis of pottery fragments, and to draw them. It presents two main advantages: (i) significant gains in time, and thus in money invested, and (ii) a fine combination of reproducibility and accuracy, accessible at different skill levels. The entire process, including 3D model acquisition, fragment orientation, and graphical illustration, should not exceed 10 minutes, no matter how complex the fragment may

be. It is not limited to wheel-turned pottery, and can process a vast range of pottery fragments (rims, body parts, and bases), increasing both the quantity and quality of information derivable from the available corpus. The success rate of the fully automatic workflow is 85% on synthetic data, and 77% on real-world archaeological fragments, but reaches almost 100% when problematic fragments are manually pre-oriented. The graphical outputs (in linear, photorealistic, or shaded modes, including scale, preservation indicator, and basic measurements) are in conformity with current standards of archaeological illustration. The graphical features, such as pottery symmetry and irregularities, which cannot be obtained by conventional methods, may provide deeper insight into many aspects of pottery production. The final output can be exported, archived, and shared, allowing further study. The approach is graphical, user-friendly, intuitive, and does not require knowledge about coding. The suite of functions integrated in the application DACORD is available in Supplementary Material S1. This tool can thus be freely improved and optimised by the archaeological community. Although the tool was developed in R, it can be adapted to a more rapid programming language and/or implemented in many systems focused on the documentation, classification, and reconstruction of archaeological pottery, to improve speed, accessibility, and operability.

Q2

A SUPPLEMENTARY MATERIALS

See the supplementary materials in the online version.

ACKNOWLEDGMENTS

We thank the museum of Lodève for allowing us access to their collections, and the master students who helped in scanning. The French Minister of Foreign Affairs is thanked for J.W.'s fellowship. We are also very grateful to Remi Laffont, Gilles Hamm, and the Bibracte Centre Archéologique Européen, and more particularly to its director, Vincent Guichard, for constant support, interest, and feedback about the tool. We are grateful to the five anonymous reviewers whose judicious comments have greatly improved the manuscript.

REFERENCES

- [1] Lesley Adkins and Roy Adkins. 1989. *Archaeological Illustration*. Cambridge University Press, Cambridge. 338
- [2] Edward B. Banning. 2006. *The Archaeologist's Laboratory: The Analysis of Archaeological Data*. Springer Science & Business Media. 339
- [3] Francesco Banterle, Barak Itkin, Matteo Dellepiane, Lior Wolf, Marco Callieri, Nachum Dershowitz, and Roberto Scopigno. 2017. VAS-ESKETCH: Automatic 3D representation of pottery from paper catalogue drawings. In *Proceedings of the 14th IAPR International Conference on Document Analysis and Recognition (ICDAR'17)*. 8. 340
- [4] Yan Cao and David Mumford. 2002. Geometric structure estimation of axially symmetric pots from small fragments. In *Structure Estimation of Axially Symmetric Pots from Small Fragments*. Article 6. 341
- [5] Winston Chang, Jow Cheng, J. J. Allaire, Yihui Xie, and Jonathan McPherson. 2017. Shiny: Web Application Framework for R. R package version 1.0.3. Retrieved October 30, 2017 from <https://CRAN.R-project.org/package=shiny>. 342
- [6] Nikolai Chernov. 2010. *Circular and Linear Regression: Fitting Circles and Lines by Least Squares*. Chapman & Hall/CRC Monographs on Statistics & Applied Probability, CRC Press. 343
- [7] Paolo Cignoni, Marco Callieri, Massimiliano Corsini, Matteo Dellepiane, Fabio Ganovelli, and Guido Ranzuglia. 2008. MeshLab: An open-source mesh processing tool. In *Proceedings of the 6th Eurographics Italian Chapter Conference*. 129–136. 344
- [8] Fernand Cohen, Zexi Liu, and Taslidere Ezgi. 2013. Virtual reconstruction of archaeological vessels using expert priors and intrinsic differential geometry information. *Computers and Graphics* 37, 1–2 (2013), 41–53. 345
- [9] Lesley Collet. 2012. *An Introduction to Drawing Archaeological Pottery*. Institute for Archaeologists, Whiteknights. 346
- [10] David B. Cooper, Andrew Willis, Stuart Andrews, Jill Baker, Yan Cao, Dongjin Han, Kongbin Kang, Weixin Kong, Frederic F. Leymarie, Xavier Orriols, Senem Velipasalar, Eileen L. Vote, Martha S. Joukowsky, Benjamin B. Kimia, David H. Laidlaw, and David Mumford. 2002. Bayesian pot-assembly from fragments as problems in perceptual grouping and geometric-learning. In *Proceedings of the 16th International Conference on Pattern Recognition*. 297–302. 347
- [11] Paolo Cortez. 2014. *Modern Optimization with R*. Springer International Publishing. 348
- [12] Brian D. Dillon. 1985. *The Student's Guide to Archaeological Illustrating*. Institute of Archaeology, University of California, Los Angeles. 349
- [13] Philippe Dolmazon. 2007. Profilograph. Retrieved October 30, 2017 from http://www.dolmazon.de/profilographie_e.htm. 350
- [14] Fabio Ganovelli, Massimiliano Corsini, Sumanta Pattanaik, and Marco Di Benedetto. 2014. *Introduction to Computer Graphics: A Practical Learning Approach*. Chapman and Hall/CRC. 351

- [15] Michael Garland and Paul S. Heckbert. 1997. Surface simplification using quadratic error metrics. In *Proceedings of the 24th Annual Conference on Computer Graphics and Interactive Techniques (SIGGRAPH'97)*. 209–216.
- [16] Wiesława Gawrysiak-Leszczyńska. 2013. *Jak Rysować Zabytki Archeologiczne*. Muzeum Archeologiczne w Biskupinie, Biskupin.
- [17] Ayelet Gilboa, Avshalom Karasik, Ilan Sharon, and Uzy Smilansky. 2004. Towards computerized typology and classification of ceramics. *Journal of Archaeological Science* 31 (2004), 681–694.
- [18] Nick Griffiths, Anne Jenner, and Christine Wilson. 1990. *Drawing Archaeological Finds: A Handbook*. University College London, London.
- [19] Maria Letizia Gualandi, Roberto Scopigno, Lior Wolf, Julian Richards, Jaume Buxeda i Garrigos, Michael Heinzelmann, Miguel Angel Hervás, Llorenç Vila, and Massimo Zallocco. 2016. ArchAIDE archaeological automatic interpretation and documentation of cERamics. In *Proceedings of the EUROGRAPHICS Workshop on Graphics and Cultural Heritage (2016)*. 4. DOI: <https://doi.org/10.2312/gch.20161408>
- [20] Radim Halíř. 1997. Estimation of the axis of rotation of fragments of archaeological pottery. In *Proceedings of the 21st Workshop of the Austrian Association for Pattern Recognition*. 175–184.
- [21] Radim Halíř. 1999. An automatic estimation of the axis of rotation of fragments of archaeological pottery: A multi-step model-based approach. In *Proceedings of the 17th International Conference in Central Europe on Computer Graphics, Visualisation and Interactive Digital Media (WSCG'99)*. 7.
- [22] Radim Halíř and Jan Flusser. 1997. Estimation of profiles of sherds of archaeological pottery. In *Proceedings of the Czech Pattern Recognition Workshop (CPRW'97)*. 126–130.
- [23] Dongjin Han and Hern-Soo Hahn. 2014. Axis estimation and grouping of rotationally symmetric object segments. *Pattern Recognition* 47, 1 (2014), 296–312.
- [24] Kateřina Hlaváčková-Schindler, Martin Kampel, and Robert Sablatnig. 2001. Fitting of a closed planar curve representing a profile of an archaeological fragment. In *Proceedings of the 2001 Conference on Virtual Reality, Archaeology, and Cultural Heritage*. 263–270.
- [25] Andrey Iones, Anton Krupkin, Mateu Sbert, and Sergey Zhukov. 2003. Fast, realistic lighting for video games. *IEEE Computer Graphics and Applications* 23, 3 (2003), 54–64.
- [26] Reiko Ishihara-Brito. 2011. Archaeological illustrations of ceramics: Drawing conventions and practices in the maya area. In *Handbook for the 1st Annual Maya at the Lago Workshop*, 2011. 16.
- [27] Martin Kampel and Robert Sablatnig. 1999. On 3D modelling of archaeological sherds. In *Proceedings of International Workshop on Synthetic-Natural Hybrid Coding and Three-Dimensional Imaging*. 95–98.
- [28] Martin Kampel and Robert Sablatnig. 1999. On estimating the position of fragments on rotational symmetric pottery. In *Proceedings of 2nd International Conference on 3-D Digital Imaging and Modelling*. 455–462.
- [29] Martin Kampel and Robert Sablatnig. 2003. An automated pottery archival and reconstruction system. *The Journal of Visualization and Computer Animation* 14 (2003), 111–120.
- [30] Martin Kampel and Robert Sablatnig. 2003. Profile-based pottery reconstruction. In *Proceedings of the Computer Vision and Pattern Recognition Workshop, 2003*. 1–6.
- [31] Martin Kampel and Robert Sablatnig. 2007. Rule based system for archaeological pottery classification. *Pattern Recognition Letters* 28, 6 (2007), 740–747.
- [32] Martin Kampel, Robert Sablatnig, and Hubert Mara. 2005. Robust 3D reconstruction of archaeological pottery based on concentric circular rills. In *Proceedings of the 6th International Workshop on Image Analysis of Multimedia Interactive Services*. 14–22.
- [33] Avshalom Karasik. 2010. A complete, automatic procedure for pottery documentation and analysis. In *Proceedings of the Computer Vision and Pattern Recognition Workshops (CVPRW'10)*. 6.
- [34] Avshalom Karasik and Uzy Smilansky. 2008. 3D scanning technology as a standard archaeological tool for pottery analysis: Practice and theory. *Journal of Archaeological Science* 35, 5 (2008), 1148–1168.
- [35] Avshalom Karasik and Uzy Smilansky. 2011. Computerized morphological classification of ceramics. *Journal of Archaeological Science* 38 (2011), 2644–2657.
- [36] Alex Méndez-Fellu and Matteu Sbert. 2009. From obscurities to ambient occlusion: A survey. *Visual Computer* 25 (2009), 181–196.
- [37] Shengqiao Li. 2011. Concise formulas for the area and volume of a hyperspherical cap. *Asian Journal of Mathematics & Statistics* 4, 1 (2011), 66–70.
- [38] Jun Liu, Mingquan Zhou, Guohua Geng, and Reziwanguli Xiamixiding. 2017. Broken pottery relic reassembling based on mixed feature vector. *Boletín Técnico/Technical Bulletin* 55, 5 (2017), 1–9.
- [39] Hubert Mara. 2009. *Pottery Plotted by Laser – 3D Acquisition for Documentation and Analysis of Symmetry of Ancient Ceramics*. Springer Berlin, 379–390.
- [40] Hubert Mara, Martin Kampel, Franco Niccolucci, and Robert Sablatnig. 2007. Ancient coins & ceramics - 3D and 2D documentation for preservation and retrieval of lost Heritage. In *Proceedings of the 2nd ISPRS International Workshop 3D-ARCH 2007: 3D Virtual Reconstruction and Visualization of Complex Architectures*. 12–13.
- [41] Hubert Mara and Julia Portl. 2013. Acquisition and documentation of vessels using high-resolution 3D-scanners. In *Neue Interdisziplinäre Dokumentations- und Visualisierungsmethoden, Corpus Vasorum Antiquorum Österreich, Beiheft 1, Verlag der Österreichischen Akademie der Wissenschaften (VÖAW)*. 25–40.

Computer-Assisted Orientation and Drawing of Archaeological Pottery • 22:17

- [42] Hubert Mara and Robert Sablatnig. 2006. Orientation of fragments of rotationally symmetrical 3D-shapes for archaeological documentation. In *Proceedings of the 3rd International 3D Data Processing, Visualization, and Transmission (3DPVT'06)*. 1064–1071. 419
- [43] Ricardo Maronna and Victor J. Yohai. 2000. Robust regression with both continuous and categorical predictors. *Journal of Statistical Planning and Inference* 89, 1–2 (2000), 197–214. 420
- [44] John C. Nash. 2014. On best practice optimization methods in R. *Journal of Statistical Software* 60, 2 (2014), 1–14. 421
- [45] John C. Nash and Ravi Varadhan. 2011. Unifying optimization algorithms to aid software system users: Optimx for R. *Journal of Statistical Software* 43, 9 (2011), 1–14. 422
- [46] Clive Orton, Paul Tyres, and Alan Vince. 1993. *Pottery in Archaeology*. Cambridge University Press, Cambridge. 423
- [47] Geoffrey Oxholm and Ko Nishino. 2013. A flexible approach to reassembling thin artifacts of unknown geometry. *Journal of Cultural Heritage* 14, 1 (2013), 51–61. 424
- [48] Georgios Papaioannou, Tobias Schreck, Anthousis Andreadis, Pavlos Mavridis, Robert Gregor, Ivan Sipiran, and Konstantinos Vardis. 2017. From reassembly to object completion: A complete systems pipeline. *Journal on Computing and Cultural Heritage* 10, 2 (2017), Article 8, 23 pages. 425
- [49] Stephen Phillips, Paul Walland, Stefano Modafferi, Michela Spagnuolo, Chiara Eva Catalano, Dominic Oldman, Ayellet Tal, Illan Shimshoni, and Sorin Hermon. 2016. GRAVITATE: Geometric and semantic matching for cultural heritage artefacts. In *Proceedings of the Eurographics Workshop on Graphics and Cultural Heritage*. 199–202. 426
- [50] Nada A. Rasheed and Md Jan Nordin. 2015. A survey of computer methods in reconstruction of 3D archaeological pottery objects. *International Journal of Advanced Research* 3, 3 (2015), 712–724. 427
- [51] Prudence M. Rice. 1987. *Pottery Analysis. A Sourcebook*. The University of Chicago Press, London. 428
- [52] Francisco Javier Melero Rus, Alejandro J. León, Francesco Contreras, and Juan Carlos Torres. 2004. A new system for interactive vessel reconstruction and drawing. *BAR International Series* 1227 (2004), 78–81. 429
- [53] Francisco Javier Melero Rus, Juan Carlos Torres, and Alejandro J. León. 2003. On the interactive 3D reconstruction of Iberian vessels. In *Proceedings of the 4th International Conference on Virtual Reality, Archaeology and Intelligent Cultural Heritage*. 71–78. 430
- [54] Robert Sablatnig, Hubert Mara, and Martin Kampel. 2005. Estimation of rotational symmetry based on concentric circular rill. In *Proceedings of the 29th Workshop of the Austrian Association for Pattern Recognition (OAGM/AAPR) and Joint Hungarian-Austrian Conference on Image Processing and Pattern Recognition*. 431
- [55] Idit Saragusti, Avshalom Karasik, Ilan Sharon, and Uzy Smilansky. 2005. Quantitative analysis of shape attributes based on contours and section profiles in artifact analysis. *Journal of Archaeological Science* 32 (2005), 841–853. 432
- [56] Stefan Schlager. 2013. *Soft-Tissue Reconstruction of the Human Nose: Population Differences and Sexual Dimorphism*. Ph.D. dissertation. Albert-Ludwigs-Universität, Freiburg. 433
- [57] Stefan Schlager. 2016. Morpho: Calculations and visualizations related to geometric morphometrics (version 2.4.1.1). Retrieved October 30, 2017 from <https://cran.r-project.org/web/packages/Morpho/Morpho.pdf>. 434
- [58] Prabodh Shirvalkar. 2016. *Analytical Drawing (Chapter 14)*. Oxford University Press, Oxford, 217–230. 435
- [59] Neil G. Smith, Avshalom Karasik, Tejaswini Naryanan, Eric S. Olson, Uzy Smilansky, and Thomas E. Levy. 2014. The pottery informatics query database: A new method for mathematic and quantitative analyses of large regional ceramic datasets. *Journal of Archaeological Method and Theory* 21 (2014), 212–250. 436
- [60] Melanie Steiner. 2005. *Approaches to Archaeological Illustration: A Handbook*. Council for British Archaeology, York. 437
- [61] RStudio Team. 2016. RStudio. Integrated Development for R. Retrieved October 30, 2017 from <http://www.rstudio.com/>. 438
- [62] R Core Team. 2016. A language and environment for statistical computing. R foundation for Statistical Computing. Retrieved October 30, 2017 from <https://www.R-project.org/>. 439
- [63] Jörg Vollmer, Robert Mencl, and Heinrich Müller. 1999. Improved Laplacian smoothing of noisy surface meshes. *Computer Graphics Forum* 18, 3 (1999), 131–138. 440
- [64] Andrew Willis and David B. Cooper. 2008. From ruins to relics: Computational reconstruction of ancient artifacts. *IEEE Signal Processing Magazine* 25 (2008), 65–83. 441
- [65] Andrew Willis, Xavier Orriols, Senem Velipasalar, Xavier Binefa, and David B. Cooper. 2000. *Extracting Axially Symmetric Geometry from Limited 3D Range Data*. Technical Report. Brown University, Brown. 442
- [66] Ben Yacoub and Christian Menard. 1997. Robust axis determination for rotational symmetric objects out of range data. In *Proceedings of the 21st AAPR Workshop*. 197–202. 443
- [67] Victor J. Yohai. 1987. High breakdown-point and high efficiency robust estimates for regression. *The Annals of Statistics* 15, 2 (1987), 642–656. 444
- [68] Kang Zhang, Wuyi Yu, Mary Manhein, Warren Waggenspack, and Xin Li. 2015. 3D fragment reassembly using integrated template guidance and fracture-region matching. In *Proceedings of the IEEE International Conference on Computer Vision*. 2138–2146. 445

Received October 2017; revised February 2018; accepted April 2018

471

Author Queries

- Q1:** AU: Please use the affiliation where the author was affiliated when the work was done in the title line. New affiliations can be noted in the page 1 notes and the author address section on page 1.
- Q2:** AU: Please verify there is supplementary materials. If there is supplementary materials please supply all source files for the supplementary materials.